JOURNAL OF CATALYSIS **176,** 102–114 (1998)
ARTICLE NO. CA982015

Acidity and Catalytic Behavior of Substituted MCM-48

H. Kosslick,*,[1] G. Lischke,† H. Landmesser,* B. Parlitz,* W. Storek,‡ and R. Fricke*

*Institut für Angewandte Chemie, Rudower Chaussee 5, D-12484 Berlin-Adlershof, Germany; †Technische Fachhochschule Wildau, Friedrich-Engels-Straße 63, D-15742 Wildau, Germany; and ‡Bundesanstalt für Materialforschung-und prüfung, BAM, Rudower Chaussee 5, D-12489 Berlin, Germany

Received July 24, 1997; revised November 10, 1997; accepted December 8, 1997

Al-, Ga-, and Fe-MCM-48 molecular sieves were synthesized and characterized by XRD, TGA, ^{29}Si-, ^{27}Al-, ^{71}Ga-MAS NMR, EPR, TPDA, and FTIR spectroscopy as well as by microcalorimetry of ammonia. Catalytic activity and selectivity were studied by the conversion of acetone. The substituting elements are, in part, incorporated into framework positions giving rise to substantial Brønsted acidity. Lewis acidity is probably generated by extra-framework species. Temperature maxima of TPDA decrease in the order: 460°C (Al) > 430°C (Ga) > 410°C (Fe). TPDA and FTIR results prove the high thermal stability of a part of acid sites. The average acidic strength of sites is lower than that observed for acidic zeolites. Nevertheless, small portions of very strong acid sites may occur. The acidic strength of Brønsted sites differs according to on the nature of the substituting element. The majority of sites has a medium-to-weak strength, but very weak and strong sites are also present. As thermal desorption shows, a broad range of Lewis acid strength is present. Samples are catalytically active and fairly stable after an initial activity loss. Fe-MCM-48 shows stable catalytic activity.

INTRODUCTION

Ordered mesoporous silicates of the M41S family, namely MCM-41 and MCM-48, were discovered recently (1, 2). They represent a new class of molecular sieve type materials which is characterized by large surface areas and by a relatively uniform shape and size of their pores. The pore diameters, which vary between 20 and 100 Å and higher (3, 4), exceed those of zeolite type molecular sieves. In addition to silicates, further meso- and nano-structured inorganic oxides have been synthesized (5–10). Owing to their unique surface properties, which combine extended surface areas with large pore sizes and volumes, these materials are assumed to be versatile catalyst supports.

Most studies published thus far deal with MCM-41. This is probably the most abundant phase appearing in the large field of synthesis parameters for M41S materials (10–12). MCM-41 has a one-dimensional hexagonally arranged pore system. The pores consist of straight tube-like channels. Recent papers report on the successful isomorphous substitution of silicon for aluminum within the framework positions by aluminum (13–16). Aluminum ions are the origin of both Brønsted and Lewis acidity and, therefore, such substituted materials are recommended for use as acid catalysts by themselves (8, 17–21).

Despite the successful development of catalytically active mesoporous MCM-41 materials, little is known about siliceous MCM-48 (22–25) and the influence exerted by isomorphous substitution on its properties (26, 27). In contrast to MCM-41, cubic MCM-48 contains two independent three-dimensional pore systems. Both pore systems are interwoven and situated in a mirror-plane position to each other.

The present paper reports on the effect of isomorphous substitution on the acidic and catalytic properties of MCM-48 silicate molecular sieves. Besides aluminum, silicon is also substituted by gallium and by iron in order to achieve a gradation of acidity. The choice of these metal ions also allows a comparison with similarly modified ZSM-type zeolites (28, 29). NMR and ESR spectroscopy are used to prove that Al, Ga, and Fe substitute tetrahedrally coordinated silicon, thus creating catalytically active sites within the walls of MCM-48. The observed Brønsted and Lewis sites cover a broad range of acidic strength. The catalytic properties are studied by the conversion of acetone which, due to its two path mechanism, is an appropriate reaction for checking the catalytic behavior of acid sites of different strength (21).

EXPERIMENTAL

Synthesis

Siliceous MCM-48 and its Al-, Ga-, and Fe-substituted species were synthesized using reaction gels of the composition: 67 $Me_2O * 1.025\ Me_2O_3 * 100\ SiO_2 * 67.7$ HDTMA Br $* 6771\ H_2O$ (HDTMABr—hexadecyltrimethylammoniumbromide). The following ingredients were used: NaOH and KOH pellets (Fluka), tetraethylorthosilicate

[1] Corresponding author. E-mail: land@aca.fta-berlin.de.

0021-9517/98 $25.00

(TEOS, Merck), aluminum pellets (Johnson Matthey), gallium (Spurenmetalle Freiberg), $Fe_2(SO_4)_3 * 5\,H_2O$ (Aldrich), HDTMABr (Merck), conc. sulfuric acid (Jenapharm Laborchemie Apolda), and deionized water. Sulfuric acid was added to increase the acidity of the iron sulfate solution to prevent polycondensation of iron hydroxide.

Metallic aluminum or gallium was dissolved in an excess of aqueous KOH solution to obtain the aluminate or the gallate, respectively. Typically, 1.265 g of alkali pellets were dissolved in 58.5 g of deionized water in a teflon cup under magnetic stirring. TEOS was slowly dropped into the clear alkaline solution under vigorous stirring. Thereafter, the HDTMABr template was added bit by bit. The necessary amount of potassium aluminate was added dropwise to the gel and stirring was continued for another 20 min to obtain a homogeneous gel. The synthesis gel was poured into teflon-lined stainless steel autoclaves and treated hydrothermally for two days at 110°C under autogeneous pressure. Then, the autoclaves were allowed to cool to room temperature (r.t.) for ca 3 h. The precipitated product was removed by centrifugation, extracted with a mixture of *i*-propanol/water, and thoroughly neutralized by as many as 15 repeated washings with deionized water and centrifugation. After drying over night at r.t., the obtained as-synthesized product was calcined for 6 h at 600°C in air (static conditions). The Si/Me ratios of calcined samples, determined by ICP-AES, were ca 32. The calcined product was ion-exchanged twice under magnetic stirring at 80°C using an aqueous 0.5 *M* solution of ammonium nitrate. Each ion exchange procedure was performed within one hour. The product was washed twice and finally dried at r.t. H, Me-MCM-48 (H-form) was obtained by thermal decomposition of the NH_4 exhanged form at 450°C for 2 h.

Characterization

XRD spectra were recorded on a Stoe automatic transmission powder diffraction system using monochromatic $CuK_{\alpha 1}$ radiation. The experimental conditions correspond to a conventional step width of 0.02°.

Thermoanalytical studies (TG-DTA) were carried out on a Setaram TGA 92-12 system. Approximately 10 mg of the samples were heated in flowing air to 800°C at a rate of 10 K/min in alumina sample holders.

^{27}Al-, ^{29}Si-, and ^{71}Ga-MAS NMR spectra were recorded on a Bruker DMX-400 spectrometer ($B_0 = 9.4$ T) at 104.3, 79.5, or 122.0 MHz, respectively. Magic angle spinning (MAS) rates were varied within a certain range, i.e.: 3.5 to 5.0 kHz with BRUKER 7 mm outer diameter standard rotors for ^{29}Si and 14 to 15 kHz for 4 mm O.D. standard rotors for ^{27}Al and ^{71}Ga. Depending on the investigated sample, the nucleus, and the attained signal/noise ratio in the registered spectra, different acquisition parameters were used. Typically, $\pi/4$ (pulse length: 6 μs) radio frequency (rf) excitation pulses and a repetition time of 25 s/scan were applied in the ^{29}Si MAS NMR with high power proton decoupling. To obtain reasonable spectra, 144 to 350 scans were accumulated. By using more than 300,000 scans and $\pi/10$ (length: 2 μs) or smaller rf excitation pulses with a repetition time of 0.4 s/scan, an excellent S/N ratio was achieved for the ^{27}Al MAS NMR spectra. Applying $\pi/10$ rf pulses (length: 0.9 μs) and a repetition time of 0.4 s/scan, 167,000 scans were necessary to obtain ^{71}Ga MAS NMR spectra. For ^{27}Al and ^{71}Ga NMR, usually 1 *M* aqueous $M(NO_3)_3$ solutions were usually chosen as external reference samples to determine the signal position δ ($[M(H_2O)_6]^{3+}$) = 0 (ppm). The chemical shifts of ^{27}Al and ^{71}Ga are not corrected for second-order quadrupole effects. For ^{29}Si NMR, the signal at −109.6 ppm of solid Q_8M_8 (cubic octamer silicic trimethyl ether) was used as an external secondary standard where ^{29}Si δ (TMS) = 0. ^{29}Si MAS NMR spectra were deconvoluted in order to obtain the positions of the lines and their relative intensities. The procedure is based on the Bruker WINFIT PC software applying pure Gaussian lines with constant line widths of 708 Hz. Al NMR spectra were deconvoluted using pure Lorentzian line shapes.

The applied single pulse excitation of the ^{71}Ga spectra was not sufficient to determine the correct position, intensity, and line shape of the signal of extra-framework Ga appearing near 0 ppm. The signals of octahedral Ga are often subject to strong quadrupolar interactions. The existence of extremely broad signals, however, would need an extraordinarily short spectrometer dead time (i.e. the time between the end of the rf pulse and the receiver opening). The experimental problems resulting from a spectrometer dead time that is too long can be overcome only by application of spin echo methods.

Acidity

A flow reactor was used for the TPDA investigations. The samples (ca 500 mg) were activated at 500°C for 1 h in a flow of helium. Subsequently, the samples were loaded with ammonia by contacting with a stream of He containing 3 vol% of ammonia at 120°C. Thermal desorption was carried out in stream of dry He at a heating rate of 10 K/min. Transmission IR studies were performed with self-supporting wafers (5–8 mg/cm^2) using a special infrared cell made from quartz glass suitable for *in situ* investigations at higher temperatures in high vacuum. The cell was connected to a high vacuum and to a gas dosing system. The spectra were recorded by a FTIR spectrometer (BIORAD FTS 60A) at 2 cm^{-1} resolution. The ammonium exchanged samples were evacuated at 30°C to remove adsorbed water. Subsequently, the samples were heated to 500°C (heating rate 5 K/min). Thermal desorption and NH_3 loading (ca 15 mbar at 100°C) were carried out in the *in situ* cell. The normalized intensity values of the Brønsted band at 1460 cm^{-1} are related to the density of the wafers.

A Calvet type microcalorimeter (SETARAM), equipped with a standard desorption device, was used to determine the differential heat of ammonia chemisorption. The samples (approx. 500 mg) were calcined overnight until constant pressure was achieved. After subsequent cooling to 150°C, they were exposed to small amounts of ammonia at this temperature. The establishment of the equilibrium of the adsorption of ammonia was followed by the measurement of the pressure after each step of adsorption.

EPR spectra of Fe-MCM-48 were recorded at room temperature and at −196°C in the X-band on a ZWG ERS-220 spectrometer. The signal of DPPH (g = 2.0036) was taken as a reference for the calculation of the g values.

Catalysis

Acetone conversion in the gas phase was performed using catalyst grains (diameter: 1.5 mm) containing 35 wt% of the H-form of the MCM-48 varieties bound with Aerosil. Grains were prepared by crushing wet-formed extruded cylinders which had been dried previously at 120°C. The reaction was performed in an integral fixed bed reactor made of stainless steel with an independently controlled two-zone heater. The mixture of the reactant gas feed was obtained by passing a nitrogen flow through a saturator held at 8.5°C giving an acetone concentration of 13.6 vol% in the gas feed. The contents of the reactant and of the products of the reaction were determined using an on-line gas-chromatograph. The analytic device was equipped with two simultaneously operating columns (a packed column with Gel II and a 30 m Hewlett–Packard column coated with 5% phenyl-methylsilicone) and a flame ionization detector coupled to a computing integrator. Prior to catalysis, the samples were dried at 120°C and finally calcined at 450°C. The catalyst mass was 1 g.

RESULTS AND DISCUSSION

Structure

XRD. The powder X-ray diffraction patterns of the siliceous and the Al-, Ga-, and Fe-substituted samples are consistent with the X-ray powder diffraction patterns of MCM-48 reported in literature (24, 27) and confirm the identity of the samples. A representative X-ray diffraction pattern of as-synthesized and calcined MCM-48 is shown in Fig. 1. The XRD pattern could be indexed in the space group *Ia3d*. The {211} reflection with the main intensity appears at approximately $2\theta = 2.1^\circ$ with a distinct shoulder at $2\theta = 2.3^\circ$, representing the {220} reflection. Further reflections of higher order, with clearly lower intensities, appear in the 2θ range between 3 and 5°. The positions of the reflections and the values of the cubic unit cell constants of Al-, Ga-, Fe-, as well as nonsubstituted siliceous MCM-48 before and after calcination are given in Table 1. The cubic

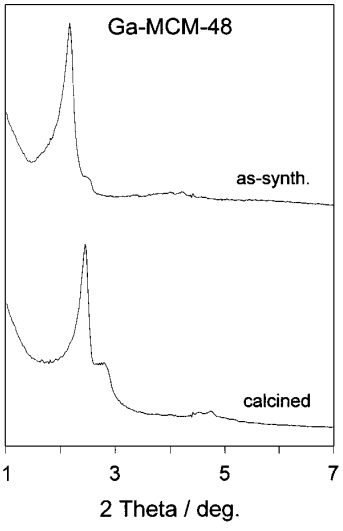

FIG. 1. XRD pattern of Ga-MCM-48.

unit cell constant a_o was calculated according to

$$a_o = d\{hkl\}\sqrt{(h^2 + k^2 + l^2)}.$$

Calcination of the template-containing as-synthesized MCM-48 causes a considerable shrinkage of about 10% of the unit cell. For the substituted samples, the positions of X-ray reflections are somewhat different. A significant influence of the isomorphous substitution, however, is not observed. This might be due to the low degree of substitution.

The shrinkage of the unit cell can be explained by the connectivity of the SiO_4 network, which is rather low in the as-synthesized samples (compare Si-NMR). Besides fourfold connected SiO_4-tetrahedra, a high amount of threefold connected species is present. Subsequent calcination causes condensation of internal SiOH groups giving rise to a contraction of the unit cell. Similar remarkable lattice contractions upon calcination are also known for MCM-41 and related molecular sieves. The metal content in the

TABLE 1

XRD Parameters of Substituted MCM-48: d-Values of Reflection, Constants of the Unit Cell, and Unit Cell Shrinkage Δ Observed after Calcination

	$d\{hkl\}$/Å					
MCM-48	{211}	{220}	{420}	{332}	a_o/Å	Δ/%
Si as-syn.	38.8	33.6	20.8	20.0	95.0	
Si calc.	34.9	30.1	18.7	17.9	84.8	10.2
Al as-syn.	43.1	39.5	22.0	21.1	105.0	
Al calc.	38.6	35.5	19.7	18.9	95.5	9.5
Ga as-syn.	40.8	35.5	22.0	20.9	100.0	
Ga calc.	36.2	31.3	19.5	18.6	88.5	11.5
Fe as-syn.	41.5	—	22.1	21.2	101.5	
Fe calc.	38.25	—	20.7	19.4	93.6	7.9

synthesis gel can be increased to Si/Me = 24 without losses of the MCM-48 structure. Only for Fe-MCM-48, did the XRD patterns show slight distortions, indicating some loss of the long range order. Framework Fe is also less stable. For reasons of convenience, comparison of the influence of isomorphous substitution on the acid and catalytic properties of MCM-48 is based on samples which were prepared with Si/Me gel ratios of 48 (Table 1). All the samples have BET surface areas of approximately 500 m^2/g.

TG-DTA. The thermoanalytical profiles confirm the structuring of silica by the template (Fig. 2). The first signal of endothermic loss in weight up to 150°C is indicative of the desorption of loosely bound interstitial water (6–7 wt%). The decomposition of the template starts at ca 150°C (ca 50 wt%) and becomes increasingly exothermic above 250°C due to the burning off in the air stream. Template decomposition proceeds through several stages, indicated by the steps in the TG curves at 250, 300, and ca 400°C. They are accompanied by three distinctive exothermic peaks in the DTA curve (Fig. 2). In comparison to free HDTMABr, the decomposition of the template starts at a higher temperature and proceeds with a low velocity over a wide temperature range. This behavior points to a true incorporation of hexadecylammonium ions into the silica matrix of MCM-48. A part of the organic compound forms coke. This is concluded from the slow burning off (weight loss) above 400°C. On Al- and Ga-MCM-48, coke formation is more pronounced (8–9%) than on the non-substituted siliceous MCM-48 (6%). Complete removal of the organic template is usually achieved at 650°C from Si-MCM-48 already at 600°C. Remarkably, in Fe-MCM-48, template oxidation is nearly complete at already 500°C, although this sample contains acid sites which are known to shift the conversion of template to coke towards elevated temperatures. The lower temperature indicates that Fe generates oxidation sites which catalyze the burning off of coke formed during thermal template decomposition!

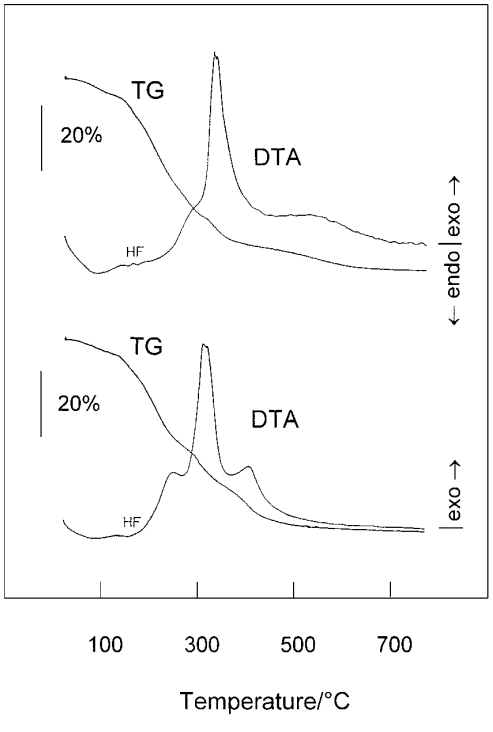

FIG. 2. Combined TG/DTA curves of as-synthesized Al-MCM-48 (top) and Fe-MCM-48 (bottom).

With substituted MCM-48, the onset temperatures of template destruction are approximately 50 K lower than with the MCM-41 samples (21). This might reflect the different dimensionalities of the pore systems: three-dimensional in MCM-48 and one-dimensional in MCM-41. The overall thermal behavior of the samples is not influenced significantly by the isomorphous substitution.

Si-NMR. The ^{29}Si MAS NMR spectra of any of the Si-, Al-, Ga-, or Fe-MCM-48 samples (Figs. 3 and 4) exhibit three lines with mean values of −91.3, −100.6, and −109.6 ppm with maximum mean deviations of ±1.7 ppm each. They are assigned to $(SiO)_2$–$Si(OH)_2$ (Q^2), $(SiO)_3$–SiOH (Q^3), or Si–$(SiO)_4$ (Q^4 groups) units, respectively (1, 14).

The isomorphously substituted samples show no additional peak that might indicate the presence of Si(1Me) units. The reason for the absence of this signal may be found in the low degree of substitution or in the fact that Si(1Me) signals of low intensity would hardly be observable due to the overlap with the strong signal of SiOH groups occurring at −100.6 ppm. To determine the percentages of different Si units in the frameworks (Table 2), the well-resolved spectra were deconvoluted (Fig. 4). The spectra of as-synthesized samples are dominated by the line at ca −101.5 ppm (Q^3 groups) and show significant intensities of the Q^2 line. With Fe-MCM-48, a change of the Q^2/Q^3 ratio in favor of Q^2 is observed. This shift points to additional distortions within the framework by the incorporation of the large iron atoms. ^{29}Si MAS NMR spectra of Fe-MCM-48 show only small side bands. This confirms conclusively that iron is highly dispersed and does not form large clusters. The comparatively low portion of Q^4 units is nearly constant for all substituted samples. The Q^4 portion of siliceous MCM-48 is somewhat higher. Due to steric constraints resulting from different sizes of the atoms and of the minimum intertetrahedral bond angles of the Si–O–Si and the Si–O–Me bridges, increasing substitution should render condensation within the framework more difficult. Therefore, decreasing framework connectivity can be brought about by an increasing isomorphous substitution.

Hence, MCM-48 samples are characterized by loosely interconnected SiO_4 tetrahedra. Their connectivity (approx. 50%) is distinctly lower than that of MCM-41 (approx. 60 to 70%). The low connectivity points to the fact that the

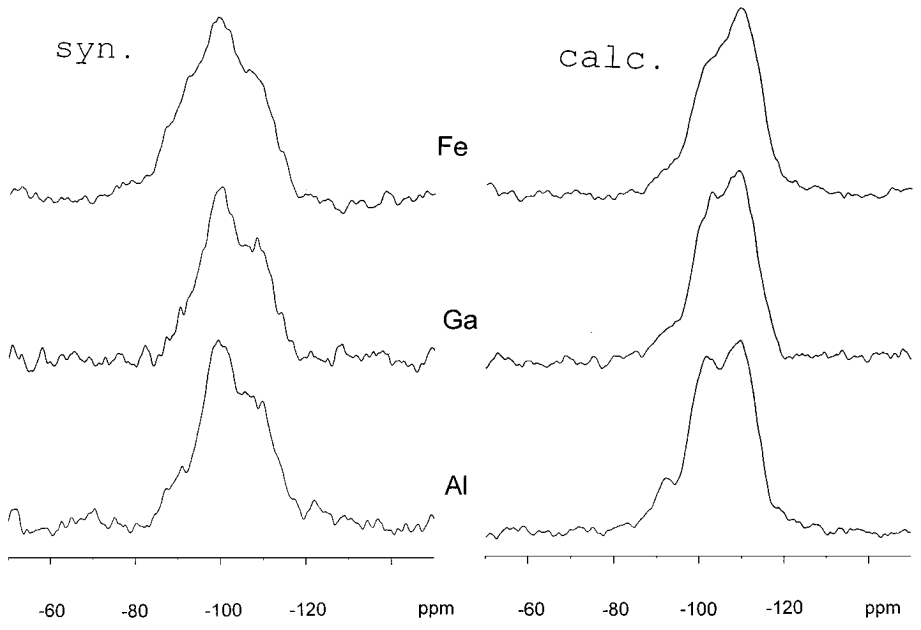

FIG. 3. ^{29}Si MAS NMR spectra of as-synthesized and calcined Al-, Ga-, Fe-MCM-48.

MCM-48 networks contain lots of internal silanol groups. The connectivity is only slightly influenced by substitution. The generally observed low connectivity implies that SiO_4 tetrahedra have only a slight chance of being arranged for condensation. Thus, the relatively narrow range of conditions for the synthesis of MCM-48-type structures may be explained. The spectrum of experimental conditions, under which MCM-41 structures are synthesized, is much broader (10).

Calcination leads to a complete change in the picture (Fig. 3). The intensities of the signals of Q^3 and Q^2 units decrease in favour of the signal of completely connected SiO_4 tetrahedra at ca −110 ppm (Table 2). Obviously, calcination leads to the condensation of nonconnected internal silanol groups. Connectivity is increased. Nevertheless, the frameworks of all the MCM-48 samples still contain a high percentage of internal silanol groups. The effect of calcination, which increases in the order Al < Ga < Fe, is definitely weaker for the pure siliceous sample.

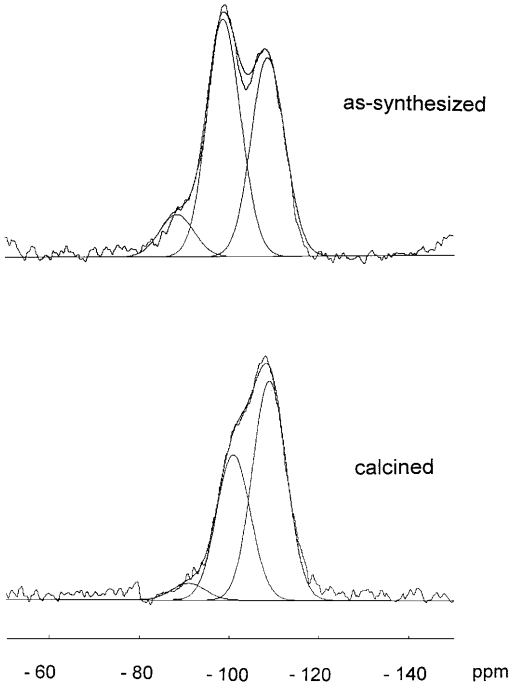

FIG. 4. Deconvoluted ^{29}Si MAS NMR spectra of as-synthesized and calcined Si-MCM-48.

TABLE 2

Connectivities of the Framework of Siliceous MCM-48 and Substituted Samples (Si/Me = 48) Determined by Line Deconvolution of ^{29}Si MAS NMR Spectra

MCM-48	Q^2 (−91.3 ppm) (%)	Q^3 (−100.6 ppm) (%)	$Q^2 + Q^3$ (%)	Q^4 (−109.6 ppm) (%)
As-syn.				
Si	8.8	49.7	58.5	41.5
Al	12.0	53.7	65.7	34.3
Ga	12.1	53.1	65.2	34.8
Fe	23.7	45.0	68.7	31.3
Calcined				
Si	4.3	38.2	42.5	57.5
Al	10.0	42.4	52.4	47.6
Ga	7.7	42.0	49.7	50.3
Fe	6.8	38.4	45.2	54.8

Note. Relative intensities of Q^n groups (%).

Considering the radii of the substituting atoms only, the reverse tendency should be expected. Besides the atomic sizes, the degrees of substitution, which decrease in the order Al > Ga > Fe, must be accounted for. The removal of Me^{3+} ions, which generates vacancies within the framework, increases the mobility of the surrounding SiO_4 tetrahedra and favors acts of condensation. Due to the low stability of the iron ions within the framework, the iron-substituted calcined sample has the highest connectivity, although it is most distorted in the as-synthesized state.

The increasing tendency to condensation within the loosely connected MCM-48 framework after calcination explains the remarkable contraction of the unit cell derived from the XRD patterns.

Isomorphous Substitution

The isomorphous substitution of silicon in the framework of MCM-48 by trivalent metal ions is directly evidenced by the ^{27}Al- and ^{71}Ga MAS NMR spectra and by the ESR spectrum of Fe-MCM-48.

Al-NMR. The ^{27}Al MAS NMR spectrum (Fig. 5) of as-synthesized Al-MCM-48 shows a strong signal at 53 ppm (assigned to tetrahedrally coordinated Al) and a weak one at approximately 5 ppm (assigned to octahedral Al). Calcination causes an increase in octahedrally coordinated Al at the expense of the tetrahedral species. The asymmetry of the tetrahedral signal at high field implies an overlap with the signal of (probably) fivefold coordinated Al appearing at approximately 32 ppm. Similar asymmetric Al NMR spectra were reported for many Al-MCM-41 molecular sieves (21, 30, 31). The percentages of the different framework and extra-framework aluminum species, derived from quantitative deconvolution of the spectra, amount to 86% of $Al^{tetr.}$ and 14% of $Al^{oct.}$ in the as-synthesized and to 62% of $Al^{tetr.}$, 22% of $Al^{pent.}$, and 16% of $Al^{oct.}$ (signal shifted to 1.3 ppm) in the calcined state. Hence, ca 80% of the isomorphously incorporated aluminum remained in the tetrahedral framework positions after calcination. These results correlate qualitatively with the TPDA data discussed below.

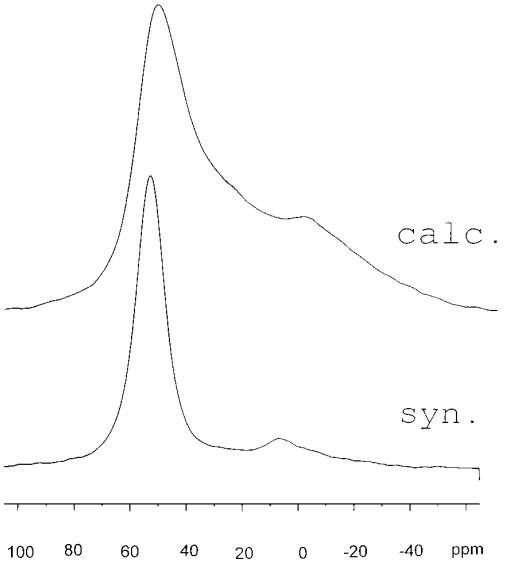

FIG. 5. ^{27}Al MAS NMR spectra of as-synthesized and calcined Al-MCM-48.

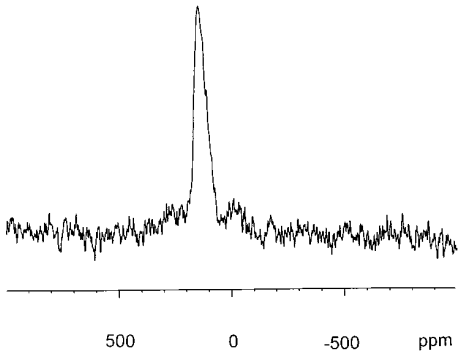

FIG. 6. ^{71}Ga MAS NMR spectrum of as-synthesized Ga-MCM-48.

Ga-NMR. In the ^{71}Ga MAS NMR spectrum of as-synthesized Ga-MCM-48 (Fig. 6), the only signal at approximately 143 ppm and a line width (fwhh) of approximately 7.8 kHz is indicative of tetrahedrally coordinated Ga (32). Again, calcination leads to a decrease in the tetrahedral species and to the appearance of octahedral gallium with a strong signal at ca 0 ppm (compare experimental part).

ESR. A variety of signals appears in the ESR spectra of as-synthesized Fe-MCM-48, depending on the degree of thermal treatment (template removal).

With the as-synthesized sample, two main signals at g = 2.0 (Signal 1) and at g = 4.3 (Signal 3) were observed (Fig. 7) and are usually assigned to octahedrally and tetrahedrally coordinated isolated Fe^{3+} ions, respectively. Upon thermal treatment in air, the intensities of original signals are drastically decreased and new signals appear (Table 3). Signal 2 (Table 3) which appears after treatment at 400°C is usually assigned to aggregated Fe^{3+} ions which already possess ferromagnetic properties (33).

Signals with g-values between approximately 6 and 8 have already been reported for iron-containing zeolite samples of various types and are commonly attributed to Fe^{3+} ions of the distorted tetrahedral or rhombohedrally distorted tetrahedral coordination (34). It is in accordance with TA and XRD findings which indicate lattice shrinkage caused by the removal of template starting already at 200°C. The assumption that the removal of the stabilizing templates also results in lattice distortions favouring the formation of tetrahedrally coordinated iron species seems reasonable.

Many ESR investigations show that this signal at g = 4.3, caused by the tetrahedrally coordinated Fe^{3+},

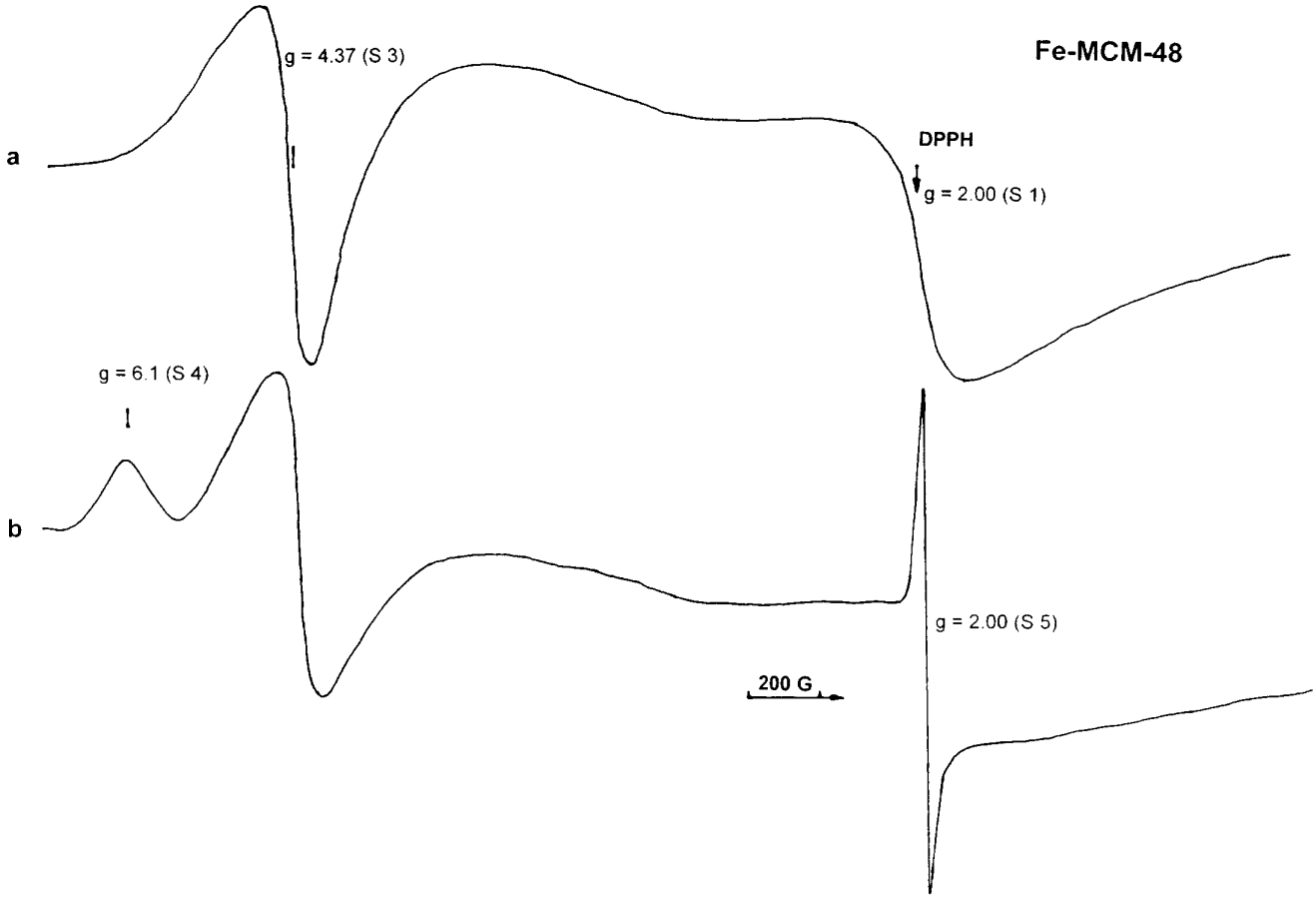

FIG. 7. ESR spectra of as-synthesized and calcined Fe-MCM-48: (a) as-synthesized; (b) after treatment in air at 300°C for 2 h (spectra recorded at liquid nitrogen temperature).

ions is visible only at the temperature of liquid nitrogen. According to our experience and that of others (35), the occurrence of the signal changes from sample to sample without any clear dependence on the conditions of its preparation. It is, therefore, assumed that the tetrahedral coordination of the respective Fe^{3+} ions is not highly stable and that even small distortions of the coordination exert a strong influence on the signal behavior. It seems

TABLE 3

Sample FeMCM-48, ESR Signal Intensities (Normalized) of the As-Synthesized State and after Treatment in Air for 2 h at Elevated Temperatures ($T_{ESR} = 20°C$)

	Signal 1		Signal 2		Signal 3		Signal 4		
Treatment (°C)	g-value	Intensity (nor)[a]	g-value	Intensity (nor)[a]	g-value	Intensity (nor)[a]	g-value	Intensity (nor)[a]	Signal 5
20	2.00	430			4.37	178			
100	2.00	134			4.37	65			
200	2.00	77			4.37	60			
300	[b]	[b]			4.36	48	6.1	17	[e]
400			[d]	[d]	4.36	30	(6.1)	[b]	[e]
500			[d]	[d]	4.36	30	(6.1)	[b]	[e]
600	2.0[c]	1200	~2.3	[d]	[b]	[b]			

[a] Intensity normalized for each signal. Intensity values not comparable between the signals!
[b] Not to be quantified due to low intensity of the signal. Signal 1: line width about 400 G.
[c] Signal 1[b]: of high intensity, line width = 200 G.
[d] Signal 2: line width > 1000 G.
[e] Signal 5: g = 2.00, line width = 11 G.

necessary to study this problem in more detail in the future.

The thermal stability of iron in the MCM-48 framework is similar to that in the ZSM-5 framework, where tetrahedrally coordinated iron ($g = 4.3$) is stable up to 550°C (36–38). Both the decrease in the signals 1 and 3 of tetrahedral and octahedral coordinated iron and the simultaneous appearance of the signal at $g = 2.3$ might be interpreted in terms of the formation of large iron clusters with ferromagnetic properties. According to the results of NMR, they, however, do not influence the ^{29}Si-NMR spectra (no coupling sidebands appear).

Acidity

Conventional TPDA. As with many zeolites (39, 40), the temperature-programmed decomposition of the NH_4 form was studied to identify Brønsted acid sites created by the incorporation of hetero atoms into the SiO_2 matrix of MCM-48. The curves of the thermal decomposition of NH_4-Al-MCM-48, NH_4-Ga-MCM-48, and NH_4-Fe-MCM-48 are shown in Fig. 8. Various types of Brønsted sites can be distinguished: sites of weak acidic strength, desorbing at 200 to 300°C, and of weak to medium strength desorbing at 280 to 350°C (shoulder). Ammonia resulting from the decomposition of NH_4^+ ions from sites of medium acidic strength is indicated by the peak with the maximum at 400 to 460°C. Unlike MCM-41 (21), MCM-48 is characterized by a more distinct distribution of Brønsted acidity. Three different types of sites are observed. It is assumed that this differentiation is the result of the specific shapes and dimensionalities of the pores, which differ substantially between both MCM varieties. The pores of MCM-48 are saddle-shaped, resulting in concave and convex curvatures, whereas the walls of MCM-41 are concave.

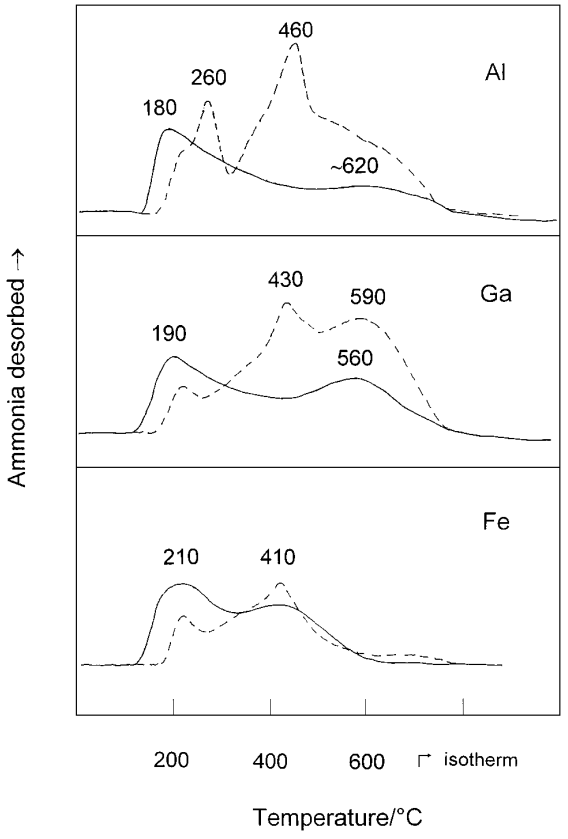

FIG. 8. Temperature-programmed desorption of ammonia from Al-, Ga-, and Fe-MCM-48: --- from NH_4-exchanged MCM-48; ——— from ammonia-loaded H,MCM-48.

The temperatures of the peak maximum rise in the order:

$$\text{Fe-MCM-48 (410°C)} < \text{Ga-MCM-48 (430°C)} < \text{Al-MCM-48 (460°C)}.$$

The same sequence was found after the incorporation of Al, Ga, or Fe into the framework of ZSM-5 (28). The shift in the temperature of the peak maxima clearly proves the increase in the acidic strength of the Brønsted sites in the order:

$$\text{Fe} < \text{Ga} < \text{Al}.$$

With Al-MCM-48 and Ga-MCM-48, the peaks of the decomposition of the NH_4^+ ions of the Brønsted sites are followed by a signal at higher temperatures. In the usual TPDA spectra (41), peaks with maxima at ca 600°C are assigned to strong Lewis acid sites. The presence of strong Lewis acidity is well known for extra-framework species in zeolites (42). Lewis sites of any acidic strength are not expected to interact with NH_4^+ ions and, therefore, should not take part in the ammonium exchange. Lewis sites of higher acidic strength, however, are able to adsorb ammonia molecules released by the decomposition of the NH_4^+ complexes of the Brønsted acid sites in a secondary act. After intermediate re-adsorption, ammonia is desorbed again from the strong acidic Lewis sites giving rise to the appearance of the high-temperature peak at above 550°C. This is why the amount of Brønsted acid sites is represented by the total area of the high-temperature signal. Fe-MCM-48 shows no unambiguous high-temperature desorption peak. This indicates that considerable amounts of strong Lewis sites do not exist. The decomposition of the NH_4^+-exchanged MCM-48 was followed by the conventional TPDA procedure to a maximum-temperature of 700°C, starting after adsorption of ammonia at 120°C. As compared with the curves of the decomposition of the NH_4^+ forms, the recorded NH_3 desorptograms of H, Al-MCM-48 and H, Ga-MCM-48 (Fig. 8) exhibit smaller amounts of Brønsted sites desorbing ammonia in the temperature range between 350 and 500°C. The loss of Brønsted sites after thermal treatment up to 700°C may also be caused by a partial dehydroxylation or by a removal of metal ions from the SiO_2 matrix and their change into octahedrally coordinated metal oxide species. The broadening of the low temperature peak of desorption

(T_{max} ca 200°C) is indicative of this transfer. The signals in the low temperature region related to weak Lewis and Brønsted sites are fairly identic for all three samples.

Like the curves of the decomposition of the NH_4^+ forms, TPDA of Al- and Ga-MCM-48 show peaks with maxima at about 600°C, attributed to desorption from very strong acidic, presumably Lewis, sites. Again, Fe-MCM-48 has no peak in the upper temperature range, but a tailing which could indicate the presence of few strong sites. The signal at 400°C is assigned to Brønsted sites of moderate strength. Its area is near to that found in the curve of the decomposition of the NH_4^+ form. This identity indicates that the incorporation of Fe ions into the SiO_2 matrix remains stable even under high temperature treatment.

It is worth mentioning that Si-MCM-48, like siliceous MCM-41, does not show any acidity. The internal silanol groups of different origin, i.e. terminal, geminal, and hydrogen bridged, are not acidic (43).

FTIR. In order to obtain more detailed information about the nature of the different peaks observed in the conventional TPDA runs, isomorphously substituted MCM-48 samples were investigated by Fourier transform infrared spectroscopy. In the FTIR difference spectra of ammonium ion-exchanged MCM-48 recorded after careful drying, evacuation, and heating to 100°C, only one band at 1460 cm^{-1} appears in the range of N–H deformation vibrations. This band characteristic of the ammonium ion (44), proves the presence of Brønsted sites and confirms the substitution of tetrahedral silicon of the framework by Al, Ga, or Fe. The normalized intensities of this band decrease in the order:

$$Ga > Al > Fe.$$

FTIR-TPDA curves of the 1460 cm^{-1} band were calculated from the decreased intensities of the absorbances observed between two sequential spectra recorded upon heating in vacuum (Fig. 9). Ammonia is desorbed from the Brønsted sites at temperatures between 200 and 400°C indicating a relatively high acidic strength of these sites. The maximum temperatures of desorption in vacuum increase in the order:

$$240 > 260 > 300°C$$

for Fe-, Ga-, or Al-MCM-48, respectively. For comparison, the desorption maximum for HY zeolite lies at ca 260°C (45).

Surprisingly, new bands at 1610 and 1300 cm^{-1}, assigned to deformation modes, arise during the thermal desorption run. They are assigned to ammonia adsorbed at Lewis acid sites (44–45). As assumed above, ammonia released, owing to the decomposition of ammonium ions of the Brønsted sites, is re-adsorbed at Lewis sites of obviously high acidic strength. The maximum of desorption from these sites is about 50 to 100°C higher than that of the Brønsted ammonia.

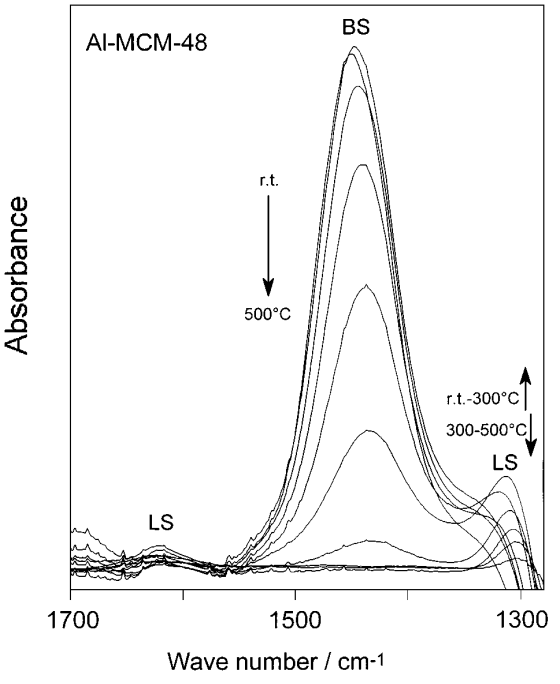

FIG. 9. FTIR difference spectra of the thermal desorption of ammonia from H,Al-MCM-48.

After a renewed adsorption of ammonia following the run of the thermal decomposition of the NH_4^+ form in the *in situ* IR cuvette, a distinct decrease in the intensities of the BS bands is observed. Thermal treatment up to 500°C results in a substantial loss of Brønsted acidity (Table 4). Ga- and Fe-MCM-48, which had originally contained a higher number of Brønsted sites than the Al-MCM-48 sample, now have the lower Brønsted acidity. It is obvious that their sites are less stable under thermal treatment. In the activated state, commonly used in catalysis, the order of concentration of Brønsted sites is changed, i.e.,

$$Al > Ga > Fe.$$

Results gained after the repeated desorption procedure up to 500°C and a subsequent second adsorption of ammonia show that the number of Brønsted sites of the activated

TABLE 4

Decrease in Brønsted Sites after Repeated Thermal Treatment up to 500°C in the Infrared Cell

Sample	Normalized intensity of the 1460 cm^{-1} band/a.u.		
	Al-MCM-48	Ga-MCM-48	Fe-MCM-48
NH_4-form	6.43	9.87	6.99
1. NH_3 adsorption	1.89	1.80	1.09
2. NH_3 adsorption	1.81	1.69	0.75

Note. Intensity values are related to the sample wafer density.

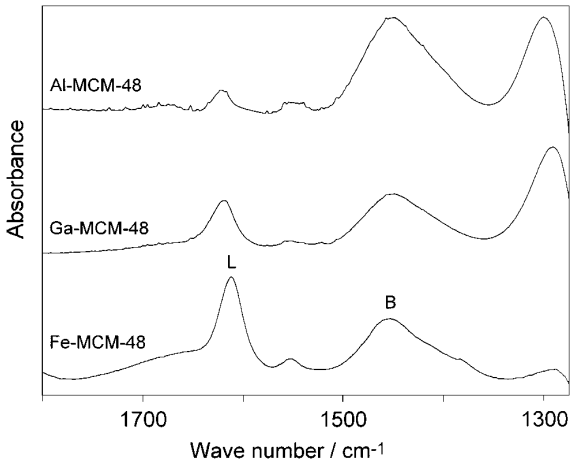

FIG. 10. FTIR spectra of ammonia adsorbed at Brønsted and Lewis sites of MCM-48 in the spectral region of NH deformation modes.

samples remains more or less the same, whereby Al-MCM-48 shows the best stability.

In the FTIR spectra of the thermally activated samples recorded after the adsorption of ammonia (Fig. 10), the additional bands at 1610 and 1300 cm^{-1}, characteristic of Lewis sites, reappear. With Al- and Ga-MCM-48, both types of Lewis sites are present, the 1300 cm^{-1} band being dominant. With Fe-MCM-48, only weaker Lewis sites (1610 cm^{-1} band) are observed. Desorption of ammonia from Lewis sites is spread over a wide temperature range up to 450°C indicating a broad distribution of acidic strengths. Furthermore, an absorbance at 1550 cm^{-1} probably occurs due to the formation of imine species via dissociative adsorption of ammonia according to (46).

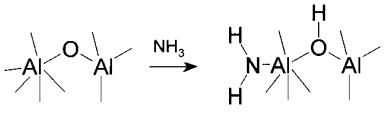

Hence, FTIR-NH_3 difference spectra recorded during the thermal desorption of ammonia from ammonium ion-exchanged samples and from ammonia loaded calcined samples are a useful tool for the unambiguous determination of the nature of the acid sites. Indeed, IR difference spectra reveal that ammonia adsorbed at strong Lewis sites (band at 1300 cm^{-1}) is thermally more stable than Brønsted ammonia characterized by the vibration band at 1450 cm^{-1}. The band of strong Lewis sites, which is more intensive with Ga-MCM-48 than with Al-MCM-48 is completely absent in the Fe-MCM-48 sample. The same tendency is observed in the conventional TPDA runs of the ammonia-loaded calcined substituted MCM-48 samples.

Since the release of ammonia already starts at a low temperature (ca 100°C), it is reasonable to assume that the low temperature peak (maximum at 200 to 250°C) in the conventional desorption profiles of ammonia of NH_4^+-exchanged samples belongs to **weak** Brønsted sites. Ammonium ions of these weak sites can be partially exchanged by washing with deionized water. The majority of the NH_4^+ ions decomposing between 300 and 400°C originates from Brønsted sites of **moderate** acid strength. The assignment of the high temperature peaks at 550 to 600°C, found in the conventional TPDA, to the desorption of ammonia from strong acid Lewis sites is confirmed by the FTIR results.

Microcalorimetry. The determination of the heat of chemisorption Q of ammonia, depending on the loading, allow us to estimate the acidic strength of acid sites in molecular sieves as well (21, 40, 41, 45). A qualitative comparison of the acidity of different types of molecular sieves can be based on the initial heat of adsorption (chemisorption) of ammonia Q_0. Values higher than 80 kJ/mol are attributed to Brønsted sites; non-acidic sites reach 40–60 kJ/mole only. The experimentally determined Q_0 values of H,Al-, H, Ga-, and H,Fe-MCM-48 amount to 140 to 155 kJ/mole, revealing the presence of strong Brønsted sites (loading of ammonia <0.1 mmol/g). Q values fall off rapidly with increasing loading of ammonia (0.2 to 0.3 mmol/g) to 80 kJ/mole and reach 50 kJ/mmol or less at a total loading of 0.5 mmol/g (Fig. 11). Thus, most of the Brønsted sites (BS) are of low acid strength. $Si/Me_{tetr.(BS)}$ framework ratios of 55 to 80 are estimated from the amount of ammonia attributed to a heat of chemisorption higher than 80 kJ/mol. On pure siliceous MCM-48, the mean value of the heat

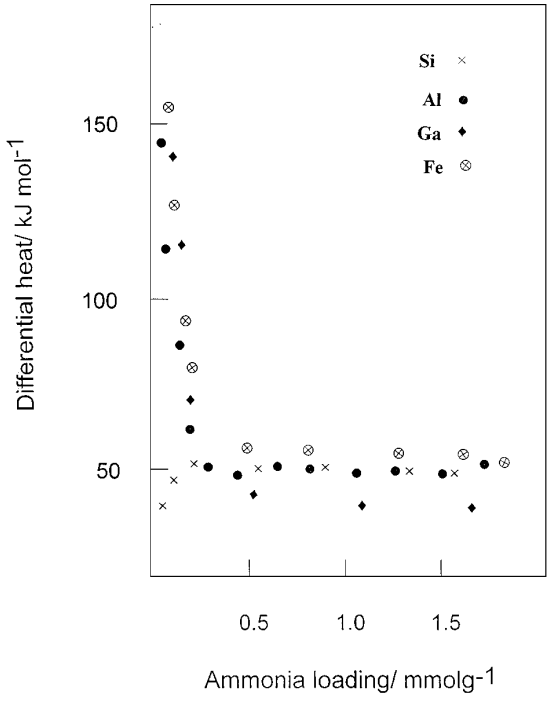

FIG. 11. Differential heats of ammonia chemisorption: ● H,Al-MCM-48; ◆ H,Ga-MCM-48; ⊗ H,Fe-MCM-48; × Si-MCM-48.

of ammonia adsorption amounts to 50 kJ/mol, i.e. internal silanol groups do not contribute to acidity as is sometimes suggested. Interestingly, its Q_0-value (40 kJ/mol) is lower than the mean value.

Catalysis

Like MCM-41 (21), Al-MCM-48, Ga-MCM-48, and Fe-MCM-48 are active catalysts in the conversion of acetone in the gas phase at about 400°C. As mentioned before, the reaction follows a two path mechanism (47). The first path is characterized by the formation of unsaturated ketones, such as phorone, followed by consecutive products, mainly C_9 aromatics. The main product of the second path is isobutene, necessarily accompanied by a certain amount of carbon dioxide.

Activity. The relative degrees of conversion of acetone obtained under standardized reaction conditions at 370°C over time on stream (TOS) are shown in Fig. 12; Al- and Ga-MCM-48 show similar activity/TOS. The initial degree of acetone conversion is relatively high, but falls off rather rapidly during the first 100 min of performance. The initial period is followed by a further but much lower decrease in activity. The shape of the activity/TOS curve of Fe-MCM-48 is clearly different. With this catalyst, the initial activity is low and increases slightly as TOS proceeds. Effects of deactivation, known from Al- and Ga-MCM-48, do not occur. Activity remains stable over a long period on stream.

Since the MCM-48 samples used in the catalytic characterization were prepared by the thermal decomposition of the NH_4^+ form of the as-synthesized products, any correlation between the catalytic behavior and the acidity has to be based on TPDA results obtained after adsorption of ammonia from the gas phase on the H-form. TPDA curves show distinct differences in the temperature region of the desorption of ammonia from Brønsted and strong acid Lewis sites.

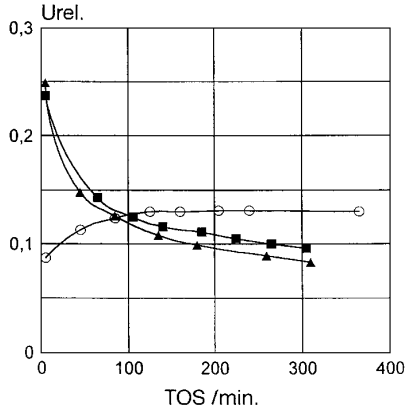

FIG. 12. Conversion of acetone-activity/time behavior temp. of reaction: 370°C, acetone concentration: 13.6 vol.-%, gas feed rate: 1.1 ml/s molar Si/Me ratio = 48.5 ± 0.3. ▲ H,Al-MCM 48; ■ H,Ga-MCM 48; ○ H,Fe-MCM 48.

TABLE 5

Catalytic Conversion of Acetone—Selectivities of the Main Products (Weight Percentage)

	Al-MCM-48	Ga-MCM-48	Fe-MCM-48
Propene	2.6	2.2	0.3
Isobutene	69.3	62.0	14.5
Mesityloxides[a]	1.6	5.4	49.7
Phorones[b]	2.4	1.9	2.7
C_9 aromatics[c]	10.2	16.7	27.5
Acetic acid	8.4	7.3	1.2

Note. Standard conditions of reaction: temp. of reaction: 370°C; catalyst volume: 6 ml; acetone concentration: 13.6 vol.% in nitrogen; gas feed rate 1.1ml/s. Average level of the degree of conversion: 15%.

[a] Sum of 2-methylpentene-2-one-4 and 2-methylpentene-1-one-4.

[b] Sum of isophorone and 2.6-dimethylhexadiene.

[c] Sum of trimethylbenzenes, predominantly mesitylene.

Both types, which are assumed to be mainly responsible for the catalytic effects, catalyze the conversion of acetone. The high stability of Fe-MCM-48, which shows no strong acidity, implies that deactivation, i.e. deposition of high boiling compounds or coke on the surface of the catalyst, is favored by strong acid, presumably Lewis, sites. They are present in remarkable amounts on only Al-MCM-48 and Ga-MCM-48. Brønsted sites of low or moderate strength, as present at Fe-MCM-48, are not able to catalyze the transformation of aromatics into highly condensed compounds (coke precursors). Catalysts can be regenerated by burning off of the coke deposits.

Selectivity. Clear differences between the samples are also observed with the selectivities of the products formed during acetone conversion. Values obtained at a stable level of conversion of acetone (ca 15% under the given conditions of reaction) are presented in Table 5.

Like Al- and Ga-MCM-41 (21), Al- and Ga-MCM-48 predominantly catalyze the second path of the reaction. The spectrum of products is dominated by isobutene. Selectivity values for the products of the first path are markedly lower. Among them, trimethylbenzenes achieve the highest selectivity. Results clearly demonstrate that the high acidic strength not only favours the formation of isobutene, but also simultaneously and effectively catalyzes the further transformation of the primary compounds of the first path of the reaction, mesityloxides and phorones, into the trimethylbenzenes and, as can be concluded from the relatively rapid deactivation, into higher condensed aromatic compounds.

Catalytic effects exerted by Fe-MCM-48 are distinctly different. Here, the first path of reaction is clearly favored. Formation of isobutene plays a secondary role. Among the compounds of the first path, mesityloxides are comparably stable. The mass ratio of the two compounds is shifted in favor of the mesityloxides, i.e., from 0.16 (for Al-MCM-48)

to 1.78 (for Fe-MCM-48). It is obvious that the subsequent reaction of the mesityloxides is catalyzed to a less extent than by the strong acid sites of Al- and Ga-MCM-48.

CONCLUSIONS

Al-, Ga-, and Fe-MCM-48 ordered mesoporous materials were synthesized and physicochemically and catalytically characterized. Their framework connectivities with respect to fourfold interconnected SiO_4 tetrahedra (Q^4 units) are low. In comparison to high-silica zeolite, e.g. ZSM-5 (48) and to MCM-41, that usually exhibit a high concentration of lattice defect sites (i.e., internal SiOH groups: Q^3 units), parent MCM-48 generally shows a lower network connectivity:

$$\text{ZSM-5 (90\% } Q^4) > \text{MCM-41 (60 to 70\% } Q^4) > \text{MCM-48 (50\% } Q^4).$$

Al, Ga, and Fe ions are incorporated into tetrahedrally coordinated framework positions. During calcination, part of the Me^{3+} is removed from their framework positions to form extra-framework species, probably located in the pore system. Nevertheless, a good portion of tetrahedrally coordinated Al, Ga, and Fe ions is stable enough to remain in their position. As is usually observed, the stability of tetrahedral substitution towards thermal treatment decreases with increasing radii of the elements.

The presence of thermally stable Brønsted sites of different strengths in the substituted MCM-48 samples is revealed by the data of acidity characterization gained by conventional TPDA, FTIR-NH_3-spectroscopy, and NH_3-microcalorimetry. The total number of stable Brønsted sites corresponding to Si/Me = 55–80 is low. The acid strength of the majority of the acidic sites is medium to weak. Some of them, however, are of high acidic strength. According to the decrease in the temperature maxima of the TPDA peaks assigned to the desorption of ammonia from Brønsted sites, acidity decreases in the order: Al > Ga > Fe. The silanol groups of the interior surface are catalytically inactive.

Additionally, Al- and Ga-MCM-48 contain weak and strong Lewis sites, from which ammonia is desorbed at 180 to 200°C and at ca 550°C, respectively. With Fe-MCM-48, strong Lewis sites are completely absent.

Brønsted and Lewis acidities, generated by the isomorphous substitution of silicon during the synthesis, give rise to a substantial catalytic activity. Differences in the nature and the acidic strength of the active sites are clearly reflected by the activity and the selectivity behavior of the catalysts in the conversion of acetone. Al- and Ga-MCM-48, which are characterized by a certain decrease in the catalytic activity in the commencing period of the reaction, predominantly catalyze the formation of isobutene, whereas Fe-MCM-48 favors the products of the competitive path, i.e. mesityloxides and C_9 aromatics. The strong Lewis acidic sites seem to be essentially responsible for the undesired formation of coke.

In principle, burning off of deposited coke offers a possibility for regenerating spent catalysts. The results show that the isomorphous substitution of some of the silicon of the framework by various metal ions may offer a way to synthesize catalysts with tailored properties. In summary, substituted MCM-48 species are promising catalytic components which are not inferior to the known MCM-41 type mesoporous molecular sieve materials.

ACKNOWLEDGMENTS

This work was partially supported by the Federal Ministry of Education, Science, Research and Technology (FRG) and the Berlin Department of Science, Research and Culture (No. 03C 3005). H.L. gratefully acknowledges a grant of the Deutsche Forschungsgemeinschaft (Fr 992/4-1).

REFERENCES

1. Kresge, C. T., Leonowicz, M. E., Roth, W. J., Vartuli, J. C., and Beck, J. S., *Nature* **359**, 710 (1992).
2. Beck, J. S., Vartuli, J. C., Rotzh, W. J., Leonowicz, M. E., Kresge, C. T., Schmitt, K. D., Chu, C. T.-W., Olson, D. H., Sheppard, E. W., McCullen, S. B., Higgins, J. B., and Schlenker, J. L., *J. Am. Chem. Soc.* **114**, 10835 (1992).
3. Yanasigawa, T., Shimizu, T., Kuroda, K., and Kato, C., *Bull. Chem. Soc. Jpn.* **63**, 988 (1990).
4. Behrens, P., *Adv. Mater.* **5**, 127 (1993).
5. Huo, Q., Margolese, D. I., Ciesla, U., Demuth, D. G., Feng, P., Gier, T. E., Sieger, P., Firouzi, A., Chmelka, B. F., Schüth, F., and Stucky, G. D., *Chem. Mater.* **6**, 1176 (1994).
6. Huo, Q., Leon, R., Petroff, P. M., and Stucky, G. D., *Science* **268**, 1324 (1995).
7. Bagshaw, S. A., Pouzet, E., and Pinnavaia, T. J., *Science* **269**, 1242 (1995).
8. Sayari, A., *Chem. Mater.* **8**, 1840 (1996).
9. Sun, T., and Ying, J. Y., *Nature* **389**, 704 (1997).
10. Raman, N. K., Anderson, M. T., and Brinker, C. J., *Chem. Mater.* **8**, 1682 (1996).
11. Göltner, C. G., and Antonietti, M., *Adv. Mater.* **9**, 431 (1997).
12. Rathousky, J., Zukal, A., Franke, O., and Schulz-Ekloff, G., *J. Chem. Soc., Faraday Trans.* **90**, 2821 (1994).
13. Corma, A., Fornes, V., Navarro, M. T., and Perez-Pariente, J., *J. Catal.* **148**, 569 (1994).
14. Chen, C. Y., Li, H. X., and Davis, M. E., *Microporous Mater.* **2**, 17 (1993)
15. Busio, M., Jänchen, J., and van Hooff, J. C. H., *Microporous Mater.* **5**, 211 (1995).
16. Tuel, A., and Gontier, S., *Chem. Mater.* **8**, 114 (1996).
17. Zhao, X. S., Millar, G. J., and Li, X. S., *Catal. Lett.* **38**, 33 (1996).
18. Roos, K., Liepold, A., Reschetilowski, W., Schmidt, R., Karlsson, A., and Stöcker, M., "Catalysis by Microporous Materials" (H. K. Beyer, H. G. Karge, I. Kiricsi, and J. B. Nagy, Eds.), p. 389. Elsevier, Amsterdam, 1995. [*in* "Stud. Surf. Sci. Catal.," Vol. 94. Liepold, A., Roos, K., Reschetilowski, W., Esculcas, A. P., Rocha, J., Philippou, A., and Anderson, W., *J. Chem. Soc., Faraday Trans.* **92**, 4623 (1996)].
19. Coustel, N., Di Renzo, F., and Fajula, F., *J. Chem. Soc., Chem. Commun.* 967 (1994).
20. Kosslick, H., Landmesser, H., and Fricke, R., *J. Chem. Soc. Faraday Trans.* **93**, 1849 (1997).

21. Kosslick, H., Lischke, G., Walther, G., Storek, W., Martin, A., and Fricke, R., *Microporous Mater.* **9**, 13 (1997).
22. Schmidt, R., Junggreen, H., and Stöcker, M., *Chem. Commun.* 875 (1996).
23. Schmidt, R., Stöcker, M., Akporiaye, D., Tørstad, E. H., and Olsen, A., *Microporous Mater.* **5**, 1 (1995).
24. Alfredsson, V., and Anderson, M. W., *Chem. Mater.* **8**, 1141 (1996).
25. Monnier, A., Schüth, F., Huo, Q., Kumar, D., Margolese, D., Maxwell, R. S., Stucky, G. D., Krishnamurty, M., Petroff, P., Firouzi, A., Janicke, M., and Chmelka, B. F., *Science* **261**, 1299 (1993).
26. Morey, M., Davidson, A., and Stucky, G., *Microporous Mater.* **6**, 99 (1996).
27. Zhang, W., and Pinnavaia, T. J., *Catal. Lett.* **38**, 261 (1996).
28. Berndt, H., Martin, A., Kosslick, H., and Lücke, B., *Microporous Mater.* **2**, 197 (1994).
29. Richter, M., Kosslick, H., Tuan, V. A., Richter-Mendau, J., Parlitz, B., Ehrhardt, K., Vorbeck, G., and Szulzewsky, K., *Ber. Bunsenges. Phys. Chem*. **96**, 586 (1992).
30. Borade, R. B., and Clearfield, A., *Catal. Lett.* **31**, 267 (1995).
31. Luan, Z., Cheng, C. F., Zhou, W. , and Klinowski, J., *J. Phys. Chem*. **99**, 1018 (1995).
32. Bayense, C. R., Kentgens, A. P. M., de Haan, J. W., van der Ven, L. J. M., and van Hooff, J. H. C., *J. Phys. Chem*. **96**, 775 (1992).
33. Derouane, E. G., Mestdagh, M., and Vielvoye, L., *J. Catal.* **33**, 169 (1974).
34. McNicol, B. D., and Pott, G. D., *J. Catal.* **25**, 223 (1972).
35. Iton, L. E., Beal, R. B., and Hodul, D. T., *J. Mol. Catal.* **21**, 151 (1983).
36. Vorbeck, G., Richter, M., Fricke, R., Parlitz, B., Schreier, E., Szulzewsky, K., and Zibrowius, B., "Catalysis and Adsorption by Zeolites" (G. Öhlmann, H. Pfeifer, and R. Fricke, Eds.), p. 631. Elsevier, Amsterdam, 1991. [in *Stud. Surf. Sci. Catal.*, Vol. 65]
37. Lazar, K., Szeleczky, A. M., Vorbeck, G., Fricke, R., Vondrova, A., and Cejka, J., *J. Radioanalyt. Nuclear Chem*. **190**, 407 (1995).
38. Lazar, K., Fricke, R., Kosslick, H., Cejka, J., Vorbeck, G., and Szeleczky, A. M., "Catalysis by Microporous Materials" (H. K. Beyer, H. G. Karge, I. Kiricsi, and J. B. Nagy, Eds.), p. 219. Elsevier, Amsterdam, 1995. [in *Stud. Surf. Sci. Catal.*, Vol. 94]
39. Karge, H. G., Dondur,V., and Weitkamp, J., *J. Phys. Chem*. **95**, 283 (1991).
40. Stach, H., Jänchen, J., Jerschkewitz, H.-G., Lohse, U., Parlitz, B., and Hunger, M., *J. Phys. Chem*. **96**, 8480 (1992).
41. Kapustin, G. I., Brueva, T. R., Klyachko, A. L., Beran, S., and Wichterlova, B., *Appl. Catal.* **42**, 239 (1988).
42. Lanh, H.D., Tuan, V. A., Kosslick, H., Parlitz, B., Fricke, R., and Völter, J., *Appl. Catal. A: General* **103**, 205 (1993).
43. Landmesser, H., Kosslick, H., Storek, W., and Fricke, R., *Solid State Ionics* **101**, 271 (1997).
44. Miessner, H., Kosslick, H., Lohse, U., Parlitz, B., and Tuan, V. A., *J. Phys. Chem*. **97**, 9741 (1993).
45. Kosslick, H., Berndt, H., Martin, A., Lanh, H. D., Miessner, H., Tuan, V. A., and Jänchen, J., *J. Chem. Soc. Faraday Trans.* **90**, 2837 (1994).
46. Shen, Y.-F., Suib, S. L., Deeba, M., and Koermer, G. S., *J. Catal.* **146**, 483 (1994).
47. Kubelkova, L., Cejka, J., Novakova, J. A., Lercher, J. A., and Jahn, E., *Z. Phys. Chem. (NF)* **168**, 231 (1990).
48. Kosslick, H., Tuan, V. A., Parlitz, B., Fricke, R., Peuker, C., and Storek, W., *J. Chem. Soc. Faraday Trans.* **89**, 1131 (1993)